# Letters

## A Fast and Highly Accurate Battery Charger With Accurate Built-In Resistance Detection

Young-Ho Jung, Jae-Hyung Jung, Hoe-Eung Jeong, Jae-Hoon Jung, Jae-Sung An, Hyun-A. Ahn, Seong-Kwan Hong, and Oh-Kyong Kwon

***Abstract*—This letter proposes a fast and highly accurate battery charger for mobile applications. The proposed battery charger accurately detects the built-in resistance (BIR) and determines the transition point from the constant-current (CC) to constant-voltage (CV) modes. It then maximizes and minimizes the durations of the CC and CV modes, respectively, thus reducing the battery charging time. In addition, the proposed charger accurately controls the charging current ($I_{BAT}$) by employing an adaptive OFF-time-controlled switching charger. The proposed battery charger was fabricated using a 0.18-$\mu$m standard CMOS process. The measurement results showed that with the use of the accurate BIR detection and adaptive OFF-time-control methods, the proposed charger reduced the total charging time by up to 41.2% and achieved $I_{BAT}$ ripple of 52 $mA_{p-p}$.**

***Index Terms*—Built-in resistance (BIR), charger, constant-current (CC) mode, constant-voltage (CV) mode, fast charging.**

### I. Introduction

LITHIUM-ION (Li-ion) batteries are widely used in mobile applications because of their small size, large capacity, and recharging capability [1]–[3]. However, they have a built-in resistance (BIR), which varies by hundreds of milliohms depending on the type of Li-ion batteries, wire connection, and printed circuit board layout [4]. In addition, the BIR is affected by the temperature variation, battery voltage, and battery usage time. In automotive applications, the electric vehicle batteries in [5] and [6] employed a complicated dynamic model including their transient behaviors to accurately estimate the state-of-charge and state-of-health variation according to the open-circuit voltage and BIR. The electric vehicle batteries in [7] adopted an ac–dc and boost converter topology, which was powered by ac input to supply a high voltage to multicell batteries.

Fig. 1(a) and (b) shows the block diagram and the charging profile of the conventional battery charging system, respectively. As shown in Fig. 1(a), the Li-ion battery can be modeled with a capacitor ($C_{CELL}$) and a resistor ($R_{BIR}$) in series, where the input of the battery charging system ($V_{IN}$) charges a battery using a battery charging current ($I_{BAT}$). The battery voltage ($V_{BAT}$) is equal to the sum of the voltage across the $R_{BIR}$ ($V_{BIR}$) and voltage charged at $C_{CELL}$ ($V_{CELL}$). Due to the characteristics of the $R_{BIR}$ and $C_{CELL}$ [1], Li-ion batteries are generally charged as depicted in the charging profile of Fig. 1(b) [2]–[4], which consists of trickle-current (TC), constant-current (CC), and constant-voltage (CV) modes. Each mode has different values of $I_{BAT}$ according to $V_{BAT}$. When $V_{BAT}$ is lower than a minimum rated voltage ($V_{TC}$), the battery charger operates in the TC mode, and the battery is charged by a trickle charging current ($I_{TC}$). When the $V_{BAT}$ is higher than $V_{TC}$ and lower than a maximum rated voltage ($V_{FULL}$), the charger operates in the CC mode with a maximum $I_{BAT}$ ($I_{CC}$) of 1 C-rate [3], which is defined as a CC that fully charges a battery in 1 h. When $V_{BAT}$ reaches $V_{FULL}$, the battery charger starts operating in the CV mode and the $V_{CELL}$ gradually approaches $V_{FULL}$. However, it is difficult to accurately determine the transition point from the CC to CV modes due to the varying BIR.

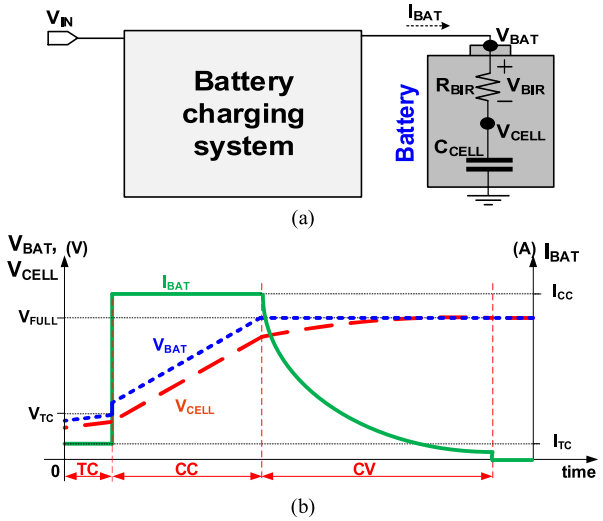


Fig. 1. (a) Block diagram and (b) charging profile of the conventional battery charging system.

Several research works on the BIR of the battery [4], [8]–[9] have been carried out in an attempt to accurately detect the BIR

Manuscript received January 22, 2018; revised March 16, 2018; accepted April 23, 2018. Date of publication April 25, 2018; date of current version September 28, 2018. *(Corresponding author: Oh-Kyong Kwon.)*

The authors are with Hanyang University, Seoul 04763, South Korea (e-mail:

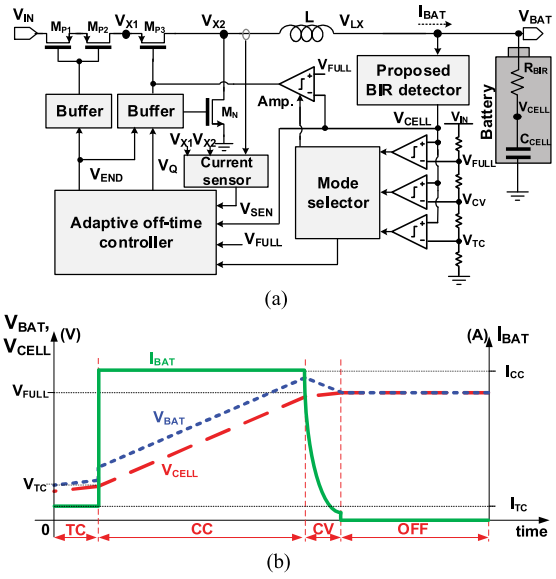


Fig. 2. (a) Block diagram and (b) charging profile of the proposed battery charger with a battery.

and determine the transition point from the CC to CV modes. The charger using one-time detection in [4] could not accurately detect the BIR because the BIR varied according to the charging time. The charger in [8] performed a complex calculation of the BIR using many variables such as an inductance value, $I_{BAT}$ change, and input voltage, while still resulting in an inaccurate BIR detection. The charger in [9] controlled a charging current to calculate the BIR for a digital compensation, but led to an inaccurate charging current and a BIR detection error.

In this letter, a battery charger is proposed in an attempt to achieve fast battery charging with accurate detection of the varying BIR, while maximizing and minimizing the durations of the CC and CV modes, respectively. Section II describes the architecture and operation including detailed circuit implementation of the adaptive OFF-time controller and the proposed BIR detector. In Section III, the experimental results are analyzed. Finally, conclusions are given in Section IV.

## II. Proposed Battery Charger

### A. Architecture and Operation

Fig. 2(a) shows the block diagram of the proposed adaptive OFF-time-controlled switching battery charger, which consists of one inductor ($L$), protection switches ($M_{P1}$ and $M_{P2}$), power switches ($M_{P3}$ and $M_N$), the proposed BIR detector, a mode selector, and an adaptive OFF-time controller. $M_{P1}$ and $M_{P2}$ are the protection switches that control the directional flow of $I_{BAT}$. $M_{P3}$ and $M_N$ with $L$ are used to adjust $I_{BAT}$ to $I_{TC}$ or $I_{CC}$ in the TC or CC mode, respectively, with high efficiency. The proposed BIR detector detects $V_{BAT}$ and determines $V_{CELL}$ by subtracting $V_{BIR}$ from $V_{BAT}$. The mode selector determines the TC, CC, or CV mode by comparing $V_{CELL}$ with $V_{TC}$, a reference of CV ($V_{CV}$), or $V_{FULL}$, respectively. The current sensor senses $I_{BAT}$, which is converted to the sensing voltage ($V_{SEN}$). Using $V_{SEN}$, the adaptive OFF-time controller generates a pulsewidth

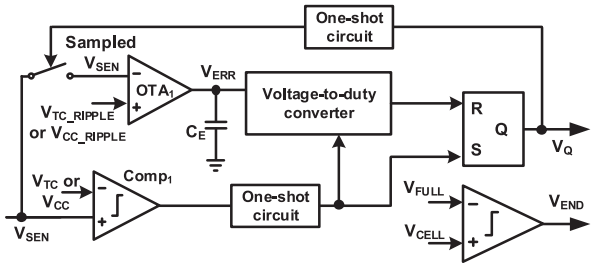


Fig. 3. Schematic of the adaptive OFF-time controller.

modulation signal ($V_Q$) to control $M_{P3}$ and $M_N$ so that $I_{BAT}$ can be accurately adjusted to $I_{CC}$ or $I_{TC}$. It also generates an ending signal ($V_{END}$) to terminate the CV mode by controlling $M_{P1}, M_{P2}, M_{P3}$, and $M_N$ and finish charging.

Fig. 2(b) shows a charging profile of the proposed charger. When $V_{CELL}$ is lower than $V_{TC}$, the proposed charger operates in the TC mode, in which an $I_{BAT}$ of $I_{TC}$ charges the battery. When $V_{CELL}$ is lower than $V_{FULL}$, the proposed charger operates in the CC mode, in which an $I_{BAT}$ of $I_{CC}$ charges the battery until $V_{CELL}$ approaches $V_{CV}$. The charger then operates in the CV mode by activating the amplifier (Amp.) to control $M_{P3}$ until $V_{CELL}$ reaches $V_{FULL}$ and then finishes the charging operation by turning OFF $M_{P1}, M_{P2}, M_{P3}$, and $M_N$. In this way, the proposed charger, respectively, maximizes and minimizes the durations of the CC and CV modes to achieve fast battery charging.

### B. Circuit Implementation

Fig. 3 shows the schematic of the adaptive OFF-time controller, which controls $I_{BAT}$ to be $I_{CC}$ or $I_{TC}$. Since the adaptive OFF-time controller has a switching ripple due to the alternate switching of $M_{P3}$ and $M_N$, it is designed to adjust its switching ripple considering the tradeoff between the ripple accuracy and the power efficiency. In the proposed charger, the adaptive OFF-time controller employs an amplifier ($OTA_1$) and a comparator ($Comp_1$) to control $V_{SEN}$ from the current sensor to be between $V_{TC}$ and $V_{TC\_RIPPLE}$ in the TC mode, and between $V_{CC}$ and $V_{CC\_RIPPLE}$ in the CC mode, where $V_{TC\_RIPPLE}$ and $V_{CC\_RIPPLE}$ are the minimum $V_{SEN}$ in the TC and CC modes, respectively. Comp1 controls the upper limit of $V_{SEN}$ by periodically comparing $V_{SEN}$ with $V_{TC}$ or $V_{CC}$ in the TC or CC mode, respectively. When $V_{BAT}$ approaches $V_{TC}$ or $V_{CC}$, the node S of the set–reset (SR) latch is activated and $V_Q$ becomes high, thus turning OFF $M_{P3}$ and turning ON $M_N$. Then, $L$ is de-energized and $I_{BAT}$ decreases, resulting in an upper limit of $I_{BAT}$ of less than $I_{TC}$ or $I_{CC}$. $OTA_1$ periodically compares the sampled $V_{SEN}$ with $V_{TC\_RIPPLE}$ or $V_{CC\_RIPPLE}$ and accumulates the error voltage of its output ($V_{ERR}$) in a capacitor, $C_E$. Then, the voltage-to-duty converter converts $V_{ERR}$ to a duty signal to control the lower limit of $V_{SEN}$. When $V_{BAT}$ approaches $V_{TC\_RIPPLE}$ or $V_{CC\_RIPPLE}$, the node R of the SR latch is activated and $V_Q$ becomes low, thus turning ON $M_{P3}$ and OFF $M_N$. Then, $L$ is energized and $I_{BAT}$ increases, resulting in a lower limit of $I_{BAT}$ of greater than $I_{TC\_RIPPLE}$ or $I_{CC\_RIPPLE}$. In this way, the adaptive OFF-time controller adjusts $I_{BAT}$ to be between $I_{TC}$ and $I_{TC\_RIPPLE}$ in the TC mode, and between $I_{CC}$ and $I_{CC\_RIPPLE}$ in the CC mode, thus minimizing the

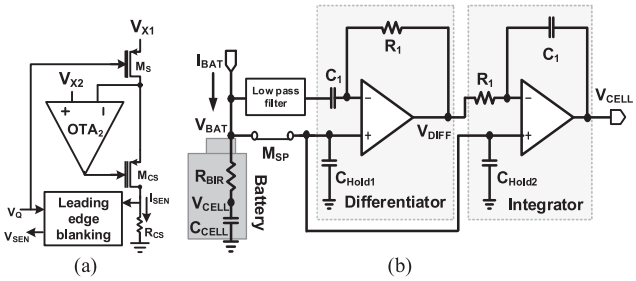


Fig. 4. Schematic of (a) the current sensor and (b) the proposed BIR detector.

ripple of $I_{\mathrm{BAT}}$ for fast battery charging. $V_{\mathrm{END}}$ is determined by comparing $V_{\mathrm{CELL}}$ and $V_{\mathrm{FULL}}$ to finish charging.

Fig 4(a) shows the current sensor used in this work, which accurately senses $I_{\mathrm{BAT}}$ and generates $V_{\mathrm{SEN}}$. The accuracy of the sensed $I_{\mathrm{BAT}}$ ($I_{\mathrm{SEN}}$) can be increased by minimizing the channel length modulation of the transistor, $\mathrm{M_{CS}}$, using the $\mathrm{OTA_2}$ and maximizing the width of the transistor, $\mathrm{M_S}$, to minimize the resistance between the source and the drain of $\mathrm{M_S}$. Furthermore, to minimize the offset of the input transistors of the $\mathrm{OTA_2}$, a common-centroid layout technique is carried out. Also, leading edge blanking is adopted to block the overshoot voltage when $\mathrm{M_S}$ is turning ON.

Fig. 4(b) shows the schematic of the BIR detector, which includes the differentiator and integrator. $V_{\mathrm{BAT}}(t)$ as a function of time is expressed as

$$V_{\mathrm{BAT}}(t) = \frac{1}{C_{\mathrm{CELL}}} \cdot \int I(t)dt + R_{\mathrm{BIR}} \cdot I(t) + V_{\mathrm{INIT}} \quad (1)$$

where $I(t)$ is an $I_{\mathrm{BAT}}$ as a function of time, and $V_{\mathrm{INIT}}$ is the initial voltage of $V_{\mathrm{BAT}}$ before starting the charging operation. In the OFF-state, $V_{\mathrm{INIT}}$ is sampled by a switch, $\mathrm{M_{SP}}$, and held in capacitors, $C_{H1}$ and $C_{H2}$, located at the positive input node of each amplifier in the differentiator and integrator, respectively. $I_{\mathrm{BAT}}$ typically varies due to a saw-tooth-shaped switching ripple of the charger. As shown in Fig. 4(b), when $V_{\mathrm{BAT}}$ is sensed by the differentiator during charging, it is averaged using a low-pass filter, and thus, $I(t)$ is assumed to be constant regardless of the switching ripple. When $I(t)$ is zero, $V_{\mathrm{CELL}}(t)$ is equal to $V_{\mathrm{BAT}}(t)$. When $I(t)$ is constant, $R_{\mathrm{BIR}} \cdot I(t)$ is canceled out by the differentiator whose output, $V_{\mathrm{DIFF}}(t)$, can be expressed as

$$\begin{aligned} V_{\mathrm{DIFF}}(t) &= -R_1C_1 \cdot \frac{dV_{\mathrm{BAT}}(t)}{dt} + V_{\mathrm{INIT}} \\ &= -R_1C_1 \cdot \frac{1}{C_{\mathrm{CELL}}} \cdot I(t) + V_{\mathrm{INIT}}. \end{aligned} \quad (2)$$

After differentiation, $V_{\mathrm{DIFF}}(t)$ is integrated by the integrator, thus canceling out $-R_1C_1$. Therefore, the output of the BIR detector as a function of time becomes $V_{\mathrm{CELL}}(t)$, which can be expressed as

$$V_{\mathrm{CELL}}(t) = \frac{1}{C_{\mathrm{CELL}}} \cdot \int I(t)dt + V_{\mathrm{INIT}}. \quad (3)$$

$R_1$ and $C_1$ in both the differentiator and the integrator are designed by adjusting their ratio and allocating them symmetrically, and thus, they are robust to the process variation.

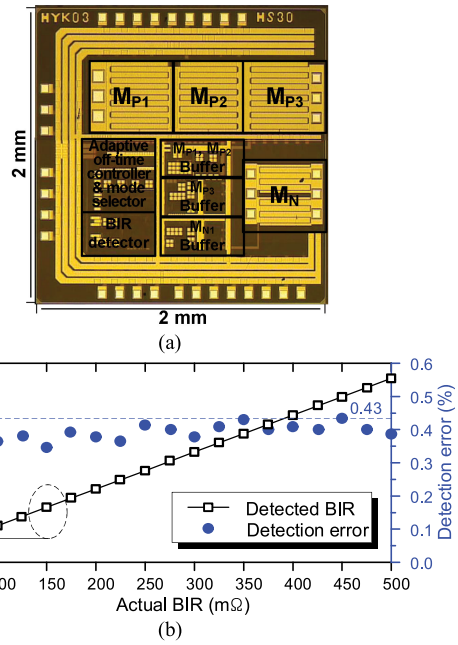


Fig. 5. (a) Chip photomicrograph and (b) measured detection error according to the BIR.

In this way, the proposed BIR detector accurately detects $V_{\mathrm{CELL}}$ as expressed in (3), thus accurately determining the transition point from the CC to CV modes.

## III. Experimental Results

The proposed fast battery charger was fabricated using a 0.18-$\mu$m standard CMOS process. In the measurement, a Li-ion battery whose $V_{\mathrm{BAT}}$ range and $I_{\mathrm{CC}}$ were 3.0–4.2 V and 2.0 A, respectively, was used. The target battery capacity in this work is 2000 mAh for mobile applications, and thus, the proposed battery charger was designed with a target battery charging current of 1 C-rate of 2.0 A for $I_{\mathrm{CC}}$, which complies with the standard charging procedure [3]. Fig. 5(a) shows the chip photomicrograph, which occupies an area of 4 mm$^2$. The prototype measurement board for measuring the $R_{\mathrm{BIR}}$ and charging profiles of $I_{\mathrm{BAT}}$, $V_{\mathrm{CELL}}$, and $V_{\mathrm{BAT}}$ was made with an inductor having an inductance value of 6.8 $\mu$H and a series-connected capacitor to endure high voltage, which has a capacitance value of 4500 F with its tolerance between –10% and 20%, and a low equivalent series resistance (ESR) value of 0.19 m$\Omega$. Fig. 5(b) shows a measured detection error of less than 0.43% over the entire BIR range between 50 and 500 m$\Omega$, which is controlled using an external resistor. The actual BIR in Fig. 5(b) was obtained by actually measuring an $R_{\mathrm{BIR}}$ using a multimeter, whereas the detected BIR was obtained by dividing the measured $V_{\mathrm{BIR}}$ by the measured $I_{\mathrm{BAT}}$ in the CC mode. Here, the measured $V_{\mathrm{BIR}}$ was obtained by subtracting the measured $V_{\mathrm{CELL}}$ of the proposed BIR detector from the measured $V_{\mathrm{BAT}}$ of the Li-ion battery. Table I shows the chip specifications and performances including a measured maximum power efficiency of 87.4%. Fig. 6(a) and (b) shows the measured charging profiles of $I_{\mathrm{BAT}}$, $V_{\mathrm{CELL}}$, and $V_{\mathrm{BAT}}$ of the chargers without and with the BIR detection and

TABLE I
CHIP SPECIFICATIONS AND PERFORMANCES

| | |
|---|---|
| **Process technology (μm)** | 0.18 |
| **Chip area (mm²)** | 4.00 |
| **L (μH)** | 6.8 |
| **$V_{BAT}$ (V)** | 3.0-4.2 |
| **Max. $I_{BAT}$ (A)** | 2.0 |
| **Max. power efficiency (%)** | 87.4 |

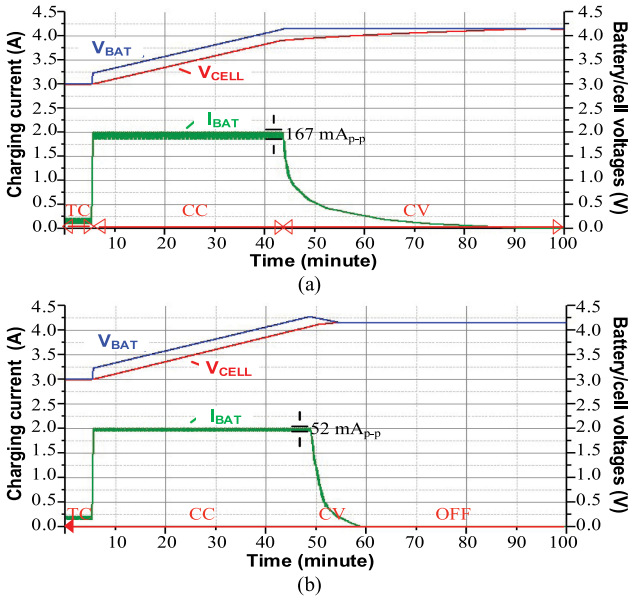


Fig. 6. Measured $I_{BAT}$, $V_{CELL}$, and $V_{BAT}$ of chargers (a) without and (b) with BIR detection and adaptive OFF-time-controlled methods.

TABLE II
COMPARISON OF THE PROPOSED CHARGER AND PREVIOUS WORKS

| | [4] | [9] | This work |
|---|---|---|---|
| **Process (μm)** | 0.35 | 0.13 | 0.18 |
| **Chip area (mm²)** | 1.10 | 1.41 | 4.00 |
| **Charger type** | Linear | Linear | Switching |
| **$V_{IN}$ (V)** | 4.5-6.5 | 4.5-6.5 | 4.5-5.5 |
| **$V_{BAT}$ (V)** | 2.5-4.2 | 2.1-4.2 | 3.0-4.2 |
| **Max. $I_{BAT}$ (A)** | 0.500 | 0.495 | 1.974 |
| **BIR detection** | One-time | Partially continuous | Continuous |
| **Total charging time saved (%)** | 20.0 | 17.1 | 41.2 |
| **Max. power efficiency (%)** | - | 83.9 | 87.4 |

OFF-time-controlled methods, showing that the durations of the CV mode were measured to be 56.2 and 8.7 min, respectively. In the CC mode of Fig. 6, where the measured $V_{BAT}$, $V_{CELL}$, and average $I_{BAT}$ are 3.572 V, 3.323 V, and 1.974 A, respectively, the $V_{BIR}$ is 0.249 V, which is obtained by ($V_{BAT} - V_{CELL}$), and thus, the detected BIR can be calculated by dividing $V_{BIR}$ by average $I_{BAT}$, which becomes 125.95 mΩ excluding the ESR. Since the actual BIR was measured to be 125.47 mΩ, the detection error is calculated to be only 0.38%, demonstrating that the proposed battery charger accurately detects the BIR, as shown in Fig. 5(b), which is almost identical to the simulation results achieved under the same measurement conditions. In addition, the measurement results in Fig. 6 demonstrate that the proposed charger charges the battery more rapidly by maximizing and minimizing the durations of the CC and CV modes, respectively, resulting in a reduction of the total charging time by 41.2%. In addition, the measured ripple of $I_{BAT}$ was reduced from 167 $mA_{p-p}$ to 52 $mA_{p-p}$. Table II shows the performance comparison of the proposed charger and previous works. Compared with previous works, the proposed charger achieved the best total charging time, saved by 41.2%, and the highest power efficiency of 87.4%.

## IV. CONCLUSION

This letter proposes a fast and highly accurate battery charger. The proposed battery charger accurately detects BIR and determines the transition point from the CC mode to the CV mode. It then reduces the charging time by maximizing and minimizing the durations of the CC and CV modes, respectively. In addition, the proposed charger accurately controls $I_{BAT}$ by employing an adaptive OFF-time-controlled switching charger, resulting in reductions of the $I_{BAT}$ ripple to 52 $mA_{p-p}$ and the total charging time by 41.2%, while having a detection error of the BIR only to be less than 0.43%. Therefore, the proposed battery is suitable for mobile devices requiring fast charging and highly accurate battery charging current.

## REFERENCES

[1] T. B. Reddy, *Linden's Handbook of Batteries*. New York, NY, USA: McGraw-Hill, 2010, pp. 2120–2214.
[2] P.-J. Liu and C.-H. Yen, "A fast-charging switching-based charger with adaptive hybrid duty cycle control for multiple batteries," *IEEE Trans. Power Electron.*, vol. 32, no. 3, pp. 1975–1983, Mar. 2017.
[3] B. D. Valle, C. T. Wentz, and R. Sarpeshkar, "An area and power-efficient analog Li-ion battery charger circuit," *IEEE Trans. Biomed. Circuits Syst.*, vol. 5, no. 2, pp. 131–137, Apr. 2011.
[4] C.-H. Lin, C.-Y. Hsieh, and K.-H. Chen, "A Li-ion battery charger with smooth control circuit and built-in resistance compensator for achieving stable and fast charging," *IEEE Trans. Circuits Syst. I, Reg. Papers*, vol. 57, no. 2, pp. 506–517, Feb. 2010.
[5] T. Mesbahi, N. Rizoug, P. Bartholomeüs, R. Sadoun, F. Khenfri, and P. Le Moigne, "Dynamic model of Li-ion batteries incorporating electrothermal and ageing aspects for electric vehicle applications," *IEEE Trans. Ind. Electron.*, vol. 65, no. 2, pp. 1298–1305, Feb. 2018.
[6] M. Bahramipanah, D. Torregrossa, R. Cherkaoui, and M. Paolone, "Enhanced equivalent electrical circuit model of lithium-based batteries accounting for charge redistribution, state-of-health, and temperature effects," *IEEE Trans. Transp. Electrific.*, vol. 3, no. 3, pp. 589–599, Sep. 2017.
[7] J.-H. Lee, J.-S. Moon, Y.-S. Lee, Y.-R. Kim, and C.-Y. Won, "Fast charging technique for EV battery charger using three-phase AC-DC boost converter," in *Proc. 37th Annu. Conf. IEEE Ind. Electron. Soc.*, Melbourne, VIC, Australia, 2011, pp. 4577–4582.
[8] R.-H. Peng *et al.*, "Switching-based charger with continuously built-in resistor detector (CBIRD) and analog multiplication-division unit (AMDU) for fast charging in Li-Ion battery," in *Proc. 39th Eur. Solid-State Circuits Conf.*, Bucharest, Romania, 2013, pp. 157–160.
[9] K. Chung, S.-K. Hong, and O.-K. Kwon, "A fast and compact charger for Li-ion battery using successive built-in resistance detection," *IEEE Trans. Circuits Syst. II, Brief Papers*, vol. 64, no. 2, pp. 161–165, Feb. 2017.